

## Article

# Thermoelectric Properties of CoCrFeNiNb<sub>x</sub> Eutectic High Entropy Alloys

Kaiming Han <sup>1</sup>, Hui Jiang <sup>1,\*</sup>, Tiandang Huang <sup>2</sup> and Mingyu Wei <sup>2</sup>

<sup>1</sup> College of Mechanical and Electronic Engineering, Shandong University of Science and Technology, Qingdao 266590, China; hankaiming2019@sdust.edu.cn

<sup>2</sup> Key Laboratory of Solidification Control and Digital Preparation Technology (Liaoning Province), School of Materials Science and Engineering, Dalian University of Technology, Dalian 116024, China; huangtd15@mail.dlut.edu.cn (T.H.); weimingyu@mail.dlut.edu.cn (M.W.)

\* Correspondence: Jianghui2019@sdust.edu.cn; Tel.: +86-532-86057207

Received: 13 August 2020; Accepted: 28 August 2020; Published: 28 August 2020



**Abstract:** Bulk CoCrFeNiNb<sub>0.45</sub> eutectic high entropy alloy (EHEA) with ultrafine-lamellar microstructure shows outstanding thermal stability. The EHEA offers opportunities for the development of thermoelectric materials. In this paper, the thermoelectric properties of a CoCrFeNiNb<sub>x</sub> ( $x = 0, 0.25$ , and  $0.45$ ) EHEA system were investigated. The results indicated that the electrical conductivity decreased with a rise in Nb content in the CoCrFeNiNb<sub>x</sub> alloys, which resulted from the increased eutectic structure and phase interface. Moreover, the thermal conductivity increased with increased Nb content at low temperature ( $T \leq 473$  K), while thermal conductivity decreased at high temperature ( $T > 573$  K). The CoCrFeNiNb<sub>0.45</sub> full eutectic high entropy alloy exhibited the lowest thermal conductivity and higher thermoelectric figure of merit (ZT) at a high temperature ( $T > 573$  K), which shows great promise for the thermoelectric application at high temperature.

**Keywords:** eutectic; high entropy alloy; electrical conductivity; thermal conductivity

## 1. Introduction

Thermoelectric (TE) materials, which can realize the conversion between heat and electricity, have received renewed attention in waste heat recoveries and TE refrigeration [1–4]. The conversion efficiency of thermoelectric materials is determined by the dimensionless figure of merit,  $ZT = (\alpha^2 \sigma T)/k$ , where  $\alpha$  is the Seebeck coefficient,  $\sigma$  is the electrical conductivity,  $k$  is the thermal conductivity, and  $T$  is the absolute temperature in Kelvin [5,6]. To maximize the ZT of a thermoelectric material, high  $\alpha$ ,  $\sigma$  and low  $k$  are required. However, it is quite difficult to achieve the above conditions simultaneously because of the competition with three parameters. Up to now, nanostructured materials changing these parameters independently lead to increase the ZT due to quantum confinement and nanostructure effects [7–9]. Although reducing the size of materials in nano-scale has been demonstrated to be an effective method to improve the thermoelectric performance, several disadvantages also exist. Firstly, many of these materials are not practical for large-scale application. Secondly, the nanostructure materials have low thermal stability, such as significant grain growth during thermal consolidation, weakening the effect of nanostructures. Therefore, for practical thermoelectric application, developing new thermoelectric materials with scalable, low cost, high thermoelectric performance and high thermal stability for extended periods of time is required.

More recently, high entropy alloys (HEAs) [10] or multi-component alloys [11] as a new type of alloys have become a research topic, which contain at least five major elements in the concentration range 5–35 at.% [12,13]. The designed alloy composition using the HEA concept can lead to the high entropy of mixing [14], particularly at elevated temperatures, and thus enhance the thermodynamic

stability of simple solid-solution phase structure. In addition, the sluggish diffusion effect in HEAs results in the crystal growing slowly, thus promoting the formation of nano-structures [15,16]. Due to their unique structures, HEAs frequently possess excellent properties [17–23]. However, solid solution HEAs possess weak liquidity and castability, which retards their industrial application. To solve the above problems, the design of eutectic high entropy alloys (EHEAs) with the characteristics of eutectic and HEA has been proposed by Lu et al. [24]. The prepared kilogram-scale AlCoCrFeNi<sub>2.1</sub> EHEA showed good liquidity, castability and good mechanical properties [25–27]. Recently, the EHEAs have been extensively studied for their eutectic composition and mechanical properties [28–37]. However, little research has focused on the physical properties of EHEAs (electrical, magnetic properties, thermal conductivity, etc.).

In our previous work, we found that ultrafine (nearly nanometer-sized)/regular lamellar eutectic structures can be obtained with a direct solidification method in CoCrFeNiNb<sub>0.45</sub> EHEA [38]. For the ultrafine eutectic structure, phonons are more strongly scattered by the interfaces, resulting in an increase in ZT. In addition, the in-situ synthetic EHEAs also have several beneficial features relative to the conventional nanostructure thermoelectric materials, such as high thermodynamic stability, low-cost method, low-energy phase boundaries and high symmetry crystal structures. Hence, the EHEAs may offer opportunities for the development of thermoelectric materials. The microstructure of the CoCrFeNiNb<sub>x</sub> ( $x = 0, 0.25$ , and  $0.45$ ) alloy system changing from a simple FCC solid solution structure ( $x = 0$ ) to hypoeutectic ( $x = 0.25$ ), then to a full eutectic structure ( $x = 0.45$ ) has been reported in our previous works [39]. So, in this paper, the thermoelectric properties of CoCrFeNiNb<sub>x</sub> ( $x = 0, 0.25$ , and  $0.45$ ) EHEAs were measured to investigate the effect of microstructure and composition on the thermoelectric properties.

## 2. Experimental

The CoCrFeNiNb<sub>x</sub> ( $x = 0, 0.25$ , and  $0.45$  denoted as Nb0, Nb0.25, and Nb0.45) eutectic high entropy alloy button ingots were prepared by co-melting elemental pure (higher than 99.95 wt. %) Co, Cr, Fe, Ni, Nb in an arc melting furnace under Ar-atmosphere. In order to obtain chemical homogeneity, the alloy ingots were melted at least five times. The microstructure was observed by scanning electron microscopy (SEM, Zeiss supra 55, Oberkochen, Germany) and transmission electron microscopy (TEM, JEOL-2100, JEOL, Japan). The specific electrical resistivity ( $1/\sigma$ ) and Seebeck coefficients ( $\alpha$ ) were measured by Namicro-3 from Wuhan Joule Yacht Science Technology Co., Ltd. with a sample dimension of  $2.5 \text{ mm} \times 2.5 \text{ mm} \times 12 \text{ mm}$ . Measurements were performed from room temperature to  $800^\circ\text{C}$  ( $28^\circ\text{C}$ ,  $100^\circ\text{C}$ ,  $200^\circ\text{C}$ ,  $300^\circ\text{C}$ ,  $400^\circ\text{C}$ ,  $500^\circ\text{C}$ ,  $600^\circ\text{C}$ ,  $700^\circ\text{C}$  and  $800^\circ\text{C}$ ) under vacuum condition. The disk samples with a dimension of  $\Phi 12.7 \text{ mm} \times 2.5 \text{ mm}$  were cut from alloy ingots and then grinded and polished to obtain a smooth surface before the thermal conductivity test. Thermal conductivity ( $k$ ) was evaluated using NETZSCH LFA 427 (Ruixuan Electronic Technology, Shanghai, China) by measuring thermal diffusivity ( $D$ ) and using the formula  $k = D \cdot \rho \cdot C_p$ . The geometrical density  $\rho$  was directly measured and heat capacity  $C_p$  was measured via STA449F1 from NETZSCH (Shanghai, China). The thermal conductivity of the alloys was measured between room temperature and  $550^\circ\text{C}$ , and the interval was kept at  $100^\circ\text{C}$ .

## 3. Results and Discussion

In our previous works, the microstructures of the CoCrFeNiNb<sub>x</sub> ingots were investigated as shown in Figure 1a–f [38,39]. Results indicated the microstructure changed from simple FCC solid structure ( $x = 0$ ) to hypoeutectic with the primary FCC phase ( $x = 0.25$ ) then to eutectic and finally ( $x = 0.45$ ). For the bulk CoCrFeNiNb<sub>0.45</sub> eutectic alloy, regular cellular eutectic containing ultrafine (nearly nanometer-sized)/regular lamellar eutectic structure can be observed. The highly uniform nanometer-sized material is rarely obtained using conventional casting. This provided an opportunity for the industrial application of the nanostructured material.

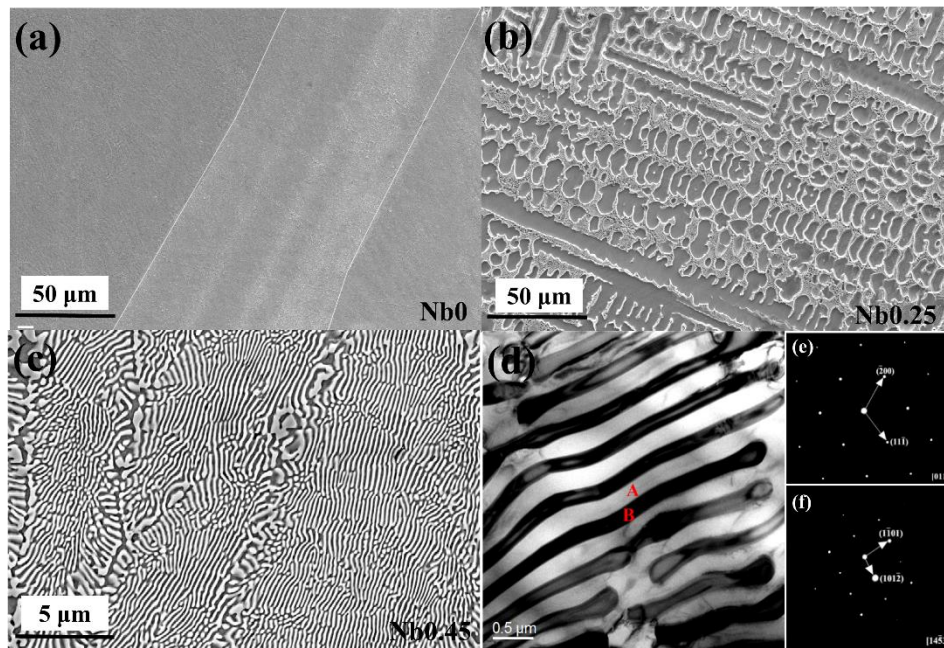


**Figure 1.** (a–c) SEM images of the CoCrFeNiNb<sub>x</sub> eutectic high entropy alloys (EHEAs), (d–f) TEM image of the CoCrFeNiNb<sub>0.45</sub> EHEAs [38,39].

Nanostructured materials have recently attracted a lot of attention for improving the performance of thermoelectric materials [40]. Thus, we present the investigation of the thermoelectric properties of CoCrFeNiNb<sub>x</sub> alloys in this paper. The temperature-dependent electrical conductivity ( $\sigma$ ) is shown in Figure 2. The specific electrical conductivity values are listed in Table 1. From the electrical conductivity data, we observed that the CoCrFeNi alloy without Nb element possesses higher electrical conductivity ( $\sigma$ ) values than that of CoCrFeNiNb<sub>x</sub> ( $x = 0.25, 0.45$ ) alloy with different Nb content at all the test temperature. In addition, the electrical conductivity of the CoCrFeNiNb<sub>x</sub> ( $x = 0, 0.25$ , and  $0.45$ ) alloys decreased with an increase in the Nb element (see Figure 2). This variation reflects the effect of microstructure morphology on the electrical property. The increase in the Nb element resulted in the increase in the volume fraction of eutectic structure; correspondingly, the amounts of the two-phase eutectic interface increased. The F-S theory was proposed by Fuchs and Sondheimer [41], which revealed the effect of the external surfaces on the electrical conductivity of the thin metal films. According to the F-S theory and the two-fluid model, the moving electrons will be scattered on the surface and at grain boundaries, which will lead to a decrease in the effective electric charge density and a decrease in electrical conductivity. In addition, the Nb element with a larger atomic radius relative to the other composition elements (the radius of Nb is 1.47 Å, the radii of the Co, Cr, Fe, and Ni elements are 1.25, 1.28, 1.26, 1.24 Å) was added into CoCrFeNi alloy causing large lattice strain. This led to a decreased carrier mobility and thus decreased electrical conductivity. With increasing temperature, the electrical conductivity decreased linearly in all the CoCrFeNiNb<sub>x</sub> alloys. The trend was consistent with the electrical resistivity dependence of the temperature in metals. The dependence of electrical resistivity on the temperature [42] is often expressed as

$$A = (\rho_s - \rho_0)/\rho_0(T - T_0) \text{ or } \rho_s = \rho_0(1 + (T - T_0)A) \quad (1)$$

where  $\rho_s$  is the electrical resistivity at temperature  $T$ ,  $\rho_0$  is the electrical resistivity at room temperature  $T_0$ , and  $A$  is the temperature coefficient of resistivity.

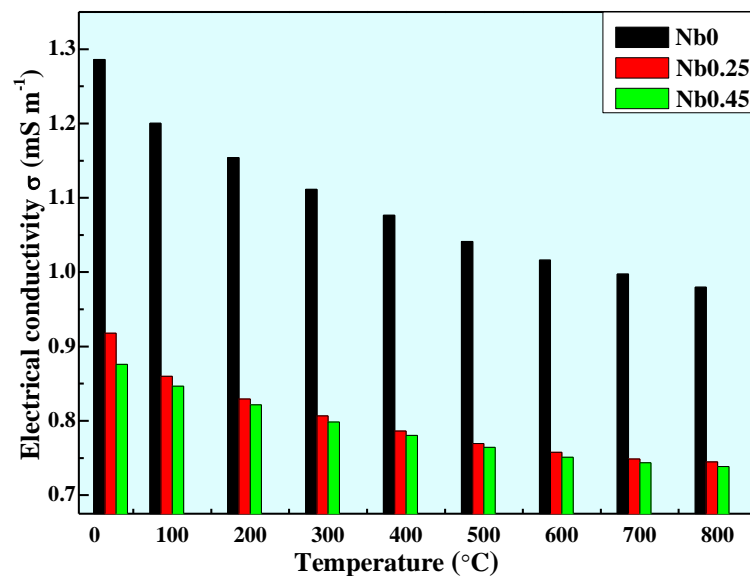


Figure 2. Electrical conductivity of the CoCrFeNiNb<sub>x</sub> (x = 0, 0.25, and 0.45) alloys.

Table 1. The specific electric resistance and electrical conductivity values of the CoCrFeNiNb<sub>x</sub> (x = 0, 0.25, and 0.45) alloys.

Alloys	Temperature	28 °C	100 °C	200 °C	300 °C	400 °C	500 °C	600 °C	700 °C	800 °C
Nb0	Electric resistance (μΩ·m)	0.7776	0.8330	0.8665	0.8996	0.9289	0.9605	0.9840	1.0026	1.0205
	Electrical conductivity (mS·m <sup>-1</sup> )	1.286	1.2004	1.1541	1.1116	1.0766	1.0411	1.0162	0.9974	0.9799
Nb0.25	Electric resistance (μΩ·m)	1.0894	1.1629	1.2056	1.2399	1.2719	1.2996	1.3202	1.3354	1.3430
	Electrical conductivity (mS·m <sup>-1</sup> )	0.918	0.8599	0.8295	0.8065	0.7862	0.7695	0.7575	0.7488	0.7446
Nb0.45	Electric resistance (μΩ·m)	1.1417	1.1810	1.2173	1.2527	1.2811	1.3082	1.3313	1.3448	1.3540
	Electrical conductivity (mS·m <sup>-1</sup> )	0.8759	0.8467	0.8215	0.7982	0.7806	0.7644	0.75112	0.7436	0.7385

However, the electrical conductivity of the CoCrFeNiNb<sub>x</sub> EHEAs was significantly higher than that of conventional binary Al-Ni eutectic [42] and some HEAs, such as the Al<sub>x</sub>CoCrFeNi (0 ≤ x ≤ 2) [43], Al<sub>x</sub>CrFeNi (x = 1.2, 1.3) [44].

Seebeck coefficients (α) of the alloys are shown in Figure 3. From Figure 3, it can be seen that the Seebeck coefficient exhibited a change trend, firstly a gradual increase from RT to 100 °C, then a sharp decrease from 100 °C to 300 °C, followed by another slight increased to 800 °C. In fact, the Seebeck coefficient [45] is more strongly correlated to the charge carrier concentration based on the Equation (2).

$$\alpha = \frac{8\pi^2 k_B^2}{3eh^2} m^* T \left( \frac{\pi}{3n} \right)^{\frac{2}{3}} \quad (2)$$

where  $k_B$  is the Boltzmann constant,  $h$  is Planck constant,  $e$  is the carrier charge,  $n$  is the carrier concentration and  $m^*$  is the density-of-states effective mass of the carrier. Thus, the raised Seebeck coefficient from 300 °C to 800 °C (see Figure 3) may come from the increase in the total number of charge carriers. From RT to 300 °C, the Seebeck coefficient lost its temperature dependency, which might be attributed to the charge carriers becoming partially localized in this temperature range.

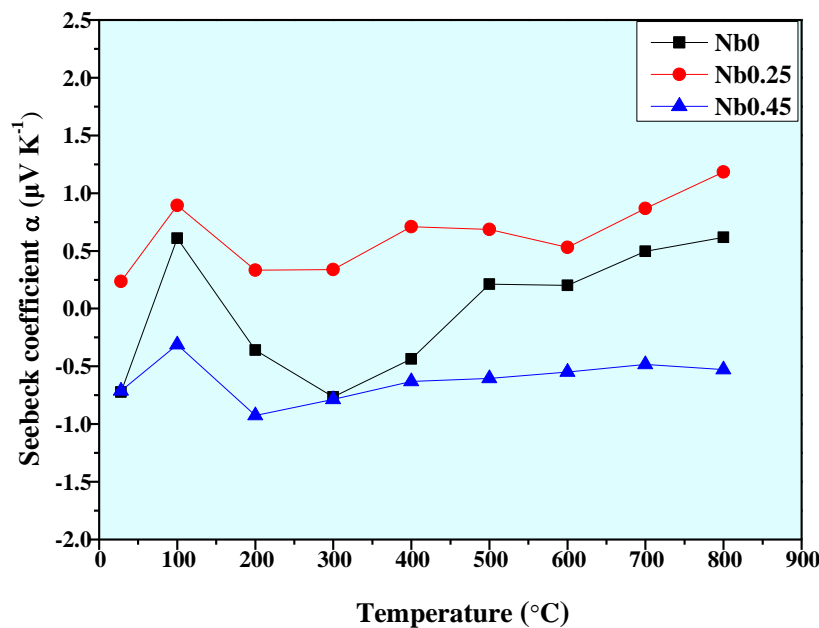


Figure 3. Seebeck coefficients ( $\alpha$ ) of the CoCrFeNiNb $_x$  ( $x = 0, 0.25$ , and  $0.45$ ) alloys.

The temperature dependence of thermal conductivity of the CoCrFeNiNb $_x$  alloys are displayed in Figure 4. It can be found that at a low temperature ( $T \leq 473$  K) the thermal conductivity increases with increased Nb content. Then, at a high temperature ( $T > 573$  K), the increased Nb content resulted in the decrease in thermal conductivity, which is in agreement with the prediction of Mingo [46]. As we know, both electrons ( $K_e$ ) and phonons ( $k_p$ ) contribute to the thermal conductivity, in which phonons usually have the majority contribution. Furthermore, the existent of interfaces and boundaries to scatter phonons is more effective than electrons. Thus, the enhanced interface and boundary phonon scattering contributed to the reduction in thermal conductivity. Moreover, the CoCrFeNiNb $_x$  ( $x = 0.25$  and  $0.45$ ) alloys exhibited a eutectic structure in situ formation, which is believed to have relatively low lattice thermal conductivity in this alloy system. In particular, the CoCrFeNiNb $_{0.45}$  alloy with full eutectic microstructure exhibited the lowest thermal conductivity at a high temperature ( $T > 573$  K). The ultrafine CoCrFeNiNb $_{0.45}$  EHEA shows outstanding microstructure thermal stability up to 1100 °C, which gives the alloy low thermal conductivity. Compared to the thermal conductivities of these HEAs and conventional metals, it can be found that the thermal conductivity of CoCrFeNiNb $_x$  alloys is lower than those of most pure metals, but is higher than those of conventional metals such as 304 stainless steel or Ni-based super-alloys [47].

The thermal conductivity of these alloys increases with the increase in temperature, which is consistent with some HEAs, stainless steel and Inconel alloy [47,48], but is opposite to most pure metals. In addition, it clear that the thermal conductivity and the electrical conductivity display an opposite temperature dependence. This increased thermal conductivity in these alloys can be explained in that the increasing temperature brought thermal expansion of the lattice and a low sensitivity of phonon concentration, which can increase the mean free path of electrons and improve the thermal conductivity.

From the thermoelectric figure of merit ZT reported in Figure 5, it is clear that the ZT values are much lower and more unsuitable for all the CoCrFeNiNb $_x$  alloys. In addition, the CoCrFeNiNb $_{0.45}$  full EHEA has the highest ZT at high temperature ( $T > 573$  K), which resulted from the lower thermal conductivity of the CoCrFeNiNb $_{0.45}$  alloy. From Figure 2, it can be found the electrical conductivity of the single phase CoCrFeNi HEAs was obviously higher than that of the CoCrFeNiNb $_{0.45}$  EHEA. The above results showed the EHEA with bimodal structure may show a great promise for thermoelectric applications.



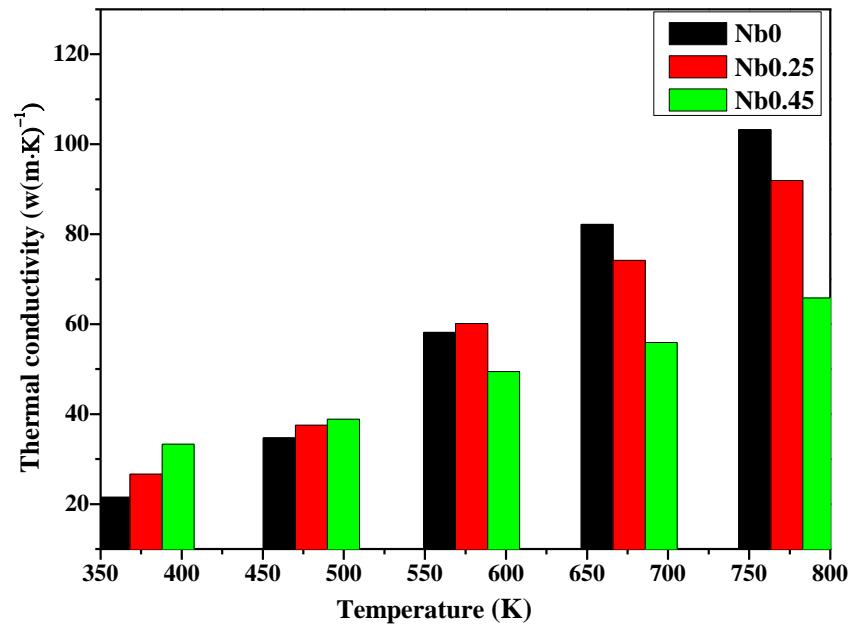


Figure 4. Thermal conductivity of the CoCrFeNiNb<sub>x</sub> (x = 0, 0.25, and 0.45) alloys.

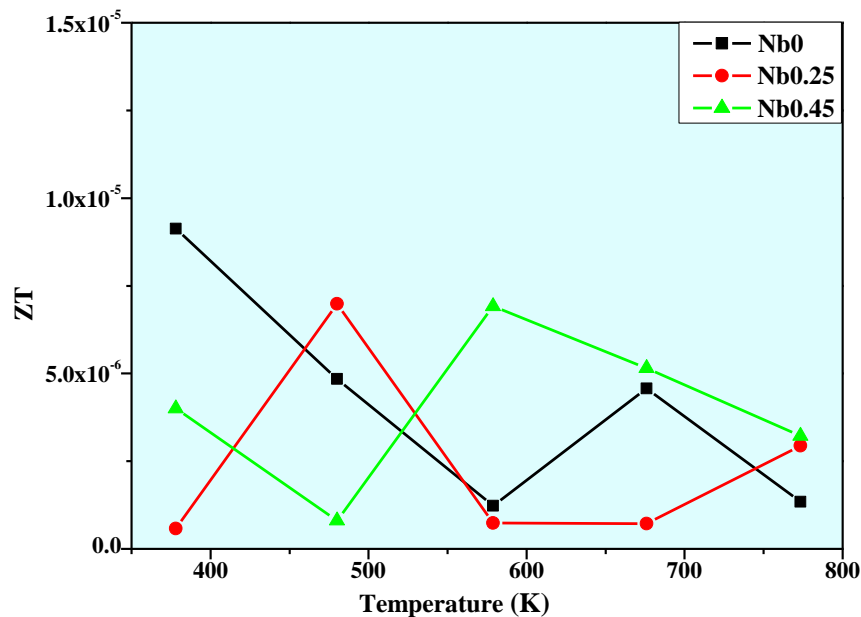


Figure 5. Thermoelectric figure of merit (ZT) of the CoCrFeNiNb<sub>x</sub> (x = 0, 0.25, and 0.45) alloys.

#### 4. Conclusions

Based upon the study of the thermoelectric properties of CoCrFeNiNb<sub>x</sub> (x = 0, 0.25, and 0.45) alloys, the following conclusions can be drawn:

- (1) With a rise in Nb content in the CoCrFeNiNb<sub>x</sub> alloys, the amounts of eutectic structure and phase interface increased, which decreased the electrical conductivity.
- (2) The thermal conductivity of the CoCrFeNiNb<sub>x</sub> alloys increases with the increase in temperature. The CoCrFeNiNb<sub>0.45</sub> full eutectic alloy exhibited the lowest thermal conductivity at a high temperature (T > 573 K).
- (3) The CoCrFeNiNb<sub>0.45</sub> full eutectic high entropy alloy has the highest ZT at high temperature (T > 573 K), which resulted from the lower thermal conductivity of the CoCrFeNiNb<sub>0.45</sub> alloy.

**Author Contributions:** Conceptualization, data curation, investigation writing—original draft, H.J. and K.H.; data curation, T.H.; writing—review and editing, M.W. All authors have read and agreed to the published version of the manuscript.

**Funding:** This work was supported by the National Natural Science Foundation of China (No. 51901116).

**Conflicts of Interest:** The authors declare no conflict of interest.

## References

- Chen, Z.; Ge, B.; Li, W.; Lin, S.; Shen, J.; Chang, Y.; Hanus, R.; Snyder, G.J.; Pei, Y. Vacancy-induced dislocations within grains for high-performance PbSe thermoelectrics. *Nat. Commun.* **2017**, *8*, 13828. [[CrossRef](#)] [[PubMed](#)]
- Alam, H.; Ramakrishna, S. A review on the enhancement of figure of merit from bulk to nano-thermoelectric materials. *Nano Energy* **2013**, *2*, 190–212. [[CrossRef](#)]
- He, J.; Tritt, T.M. Advances in thermoelectric materials research: Looking back and moving forward. *Science* **2017**, *357*, eaak9997. [[CrossRef](#)] [[PubMed](#)]
- Wolf, M.; Hinterding, R.; Feldhoff, A. High power factor vs. high  $zT$ —A Review of thermoelectric materials for high-temperature application. *Entropy* **2019**, *21*, 1058. [[CrossRef](#)]
- Stoetzel, J.; Schneider, T.; Mueller, M.M.; Kleebe, H.-J.; Wiggers, H.; Schierning, G.; Schmechel, R. Microstructure and thermoelectric properties of Si-WSi<sub>2</sub> nanocomposites. *Acta Mater.* **2017**, *125*, 321–326. [[CrossRef](#)]
- Zhang, J.; Song, L.; Pedersen, S.H.; Yin, H.; Hung, L.T.; Iversen, B.B. Discovery of high-performance low-cost n-type Mg<sub>3</sub>Sb<sub>2</sub>-based thermoelectric materials with multi-valley conduction bands. *Nat. Commun.* **2017**, *8*, 13901. [[CrossRef](#)]
- Liu, Z.; Gao, W.; Meng, X.; Li, X.; Mao, J.; Wang, Y.; Shuai, J.; Cai, W.; Ren, Z.; Sui, J. Mechanical properties of nanostructured thermoelectric materials  $\alpha$ -MgAgSb. *Scr. Mater.* **2017**, *127*, 72–75. [[CrossRef](#)]
- Chen, Z.G.; Han, G.; Yang, L.; Cheng, L.; Zou, J. Nanostructured thermoelectric materials: Current research and future challenge. *Prog. Nat. Sci. Mater.* **2012**, *22*, 535–549. [[CrossRef](#)]
- Liang, L.; Chen, G.; Guo, C.Y. Polypyrrole nanostructures and their thermoelectric performance. *Mater. Chem. Front.* **2017**, *1*, 380–386. [[CrossRef](#)]
- Yeh, J.W.; Chen, S.K.; Lin, S.J.; Gan, J.Y.; Chin, T.S.; Shun, T.T.; Tsau, C.H.; Chang, S.Y. Nanostructured high-entropy alloys with multiple principal elements: Novel alloy design concepts and outcomes. *Adv. Eng. Mater.* **2004**, *6*, 299–303. [[CrossRef](#)]
- Cantor, B.; Chang, I.T.H.; Knight, P.; Vincent, A.J.B. Microstructural development in equiatomic multicomponent alloys. *Mater. Sci. Eng. A* **2004**, *375–377*, 213–218. [[CrossRef](#)]
- Zhang, Y.; Zuo, T.T.; Tang, Z.; Gao, M.C.; Dahmen, K.A.; Liaw, P.K.; Lu, Z.P. Microstructures and properties of high-entropy alloys. *Prog. Mater. Sci.* **2014**, *61*, 1–93. [[CrossRef](#)]
- Gao, M.C.; Yeh, J.W.; Liaw, P.K.; Zhang, Y. *High Entropy Alloys Fundamentals and Applications*; Springer International Publishing: Cham, Switzerland, 2016.
- Yeh, J.W. Alloy Design strategies and future trends in high-entropy alloys. *JOM* **2013**, *65*, 1759–1771. [[CrossRef](#)]
- Beke, D.L.; Erdélyi, G. On the diffusion in high-entropy alloys. *Mater. Lett.* **2016**, *164*, 111–113. [[CrossRef](#)]
- Liu, W.H.; Wu, Y.; He, J.Y.; Nieh, T.G.; Lu, Z.P. Grain growth and the Hall–Petch relationship in a high-entropy FeCrNiCoMn alloy. *Scr. Mater.* **2013**, *68*, 526–529. [[CrossRef](#)]
- Li, Z.; Pradeep, K.G.; Deng, Y.; Raabe, D.; Tasan, C.C. Metastable high-entropy dual-phase alloys overcome the strength–ductility trade-off. *Nature* **2016**, *534*, 227–230. [[CrossRef](#)]
- Zhang, Y.; Yang, X.; Liaw, P.K. Alloy design and properties optimization of high-entropy alloys. *JOM* **2012**, *64*, 830–838. [[CrossRef](#)]
- Gludovatz, B.; Hohenwarter, A.; Catoor, D.; Chang, E.H.; George, E.P.; Ritchie, R.O. A fracture-resistant high-entropy alloy for cryogenic applications. *Science* **2014**, *345*, 1153–1158. [[CrossRef](#)]
- Stepanov, N.D.; Yurchenko, N.Y.; Sokolovsky, V.S.; Tikhonovsky, M.A.; Salishchev, G.A. An AlNbTiVZr<sub>0.5</sub> high-entropy alloy combining high specific strength and good ductility. *Mater. Lett.* **2015**, *161*, 136–139. [[CrossRef](#)]

21. Zuo, T.T.; Gao, M.C.; Ouyang, L.Z.; Yang, X.; Cheng, Y.Q.; Feng, R.; Chen, S.Y.; Liaw, P.K.; Hawk, J.A.; Zhang, Y. Tailoring magnetic behavior of CoFeMnNiX (X = Al, Cr, Ga, and Sn) high entropy alloys by metal doping. *Acta Mater.* **2017**, *130*, 10–18. [[CrossRef](#)]
22. Lu, C.; Yang, T.; Jin, K.; Gao, N.; Xiu, P.; Zhang, Y.; Gao, F.; Bei, H.; Weber, W.J.; Sun, K.; et al. Radiation-induced segregation on defect clusters in single-phase concentrated solid-solution alloys. *Acta Mater.* **2017**, *127*, 98–107. [[CrossRef](#)]
23. Shi, Y.; Yang, B.; Xie, X.; Brechtel, J.; Dahmen, K.A.; Liaw, P.K. Corrosion of Al<sub>x</sub>CoCrFeNi high-entropy alloys: Al-content and potential scan-rate dependent pitting behavior. *Corros. Sci.* **2017**, *119*, 33–45. [[CrossRef](#)]
24. Lu, Y.; Dong, Y.; Guo, S.; Jiang, L.; Kang, H.; Wang, T.; Wen, B.; Wang, Z.; Jie, J.; Cao, Z.; et al. A promising new class of high-temperature alloys: Eutectic high-entropy alloys. *Sci. Rep.* **2014**, *4*, 6200. [[CrossRef](#)] [[PubMed](#)]
25. Lu, Y.; Gao, X.; Jiang, L.; Chen, Z.; Wang, T.; Jie, J.; Kang, H.; Zhang, Y.; Guo, S.; Ruan, H.; et al. Directly cast bulk eutectic and near-eutectic high entropy alloys with balanced strength and ductility in a wide temperature range. *Acta Mater.* **2017**, *124*, 143–150. [[CrossRef](#)]
26. Wani, I.S.; Bhattacharjee, T.; Sheikh, S.; Lu, Y.P.; Chatterjee, S.; Bhattacharjee, P.P.; Guo, S.; Tsuji, N. Ultrafine-grained AlCoCrFeNi<sub>2.1</sub> eutectic high-entropy alloy. *Mater. Res. Lett.* **2016**, *4*, 174–179. [[CrossRef](#)]
27. Wani, I.S.; Bhattacharjee, T.; Sheikh, S.; Clark, I.T.; Park, M.H.; Okawa, T.; Guo, S.; Bhattacharjee, P.P.; Tsuji, N. Cold-rolling and recrystallization textures of a nano-lamellar AlCoCrFeNi<sub>2.1</sub> eutectic high entropy alloy. *Intermetallics* **2017**, *84*, 42–51. [[CrossRef](#)]
28. Lu, Y.; Dong, Y.; Jiang, H.; Wang, Z.; Cao, Z.; Guo, S.; Wang, T.; Li, T.; Liaw, P.K. Promising properties and future trend of eutectic high entropy alloys. *Scr. Mater.* **2020**, *187*, 202–209. [[CrossRef](#)]
29. Wu, Q.; Wang, Z.; Zheng, T.; Chen, D.; Yang, Z.; Li, J.; Kai, J.J.; Wang, J. A casting eutectic high entropy alloy with superior strength-ductility combination. *Mater. Lett.* **2019**, *253*, 268–271. [[CrossRef](#)]
30. Dong, Y.; Yao, Z.; Huang, X.; Du, F.; Li, C.; Chen, A.; Wu, F.; Cheng, Y.; Zhang, Z. Microstructure and mechanical properties of AlCo<sub>x</sub>CrFeNi<sub>3-x</sub> eutectic high-entropy-alloy system. *J. Alloy. Compd.* **2020**, *823*, 153886. [[CrossRef](#)]
31. Wu, M.; Munroe, P.R.; Baker, I. Martensitic phase transformation in a f.c.c./B2 FeNiMnAl alloy. *J. Mater. Sci.* **2016**, *51*, 7831–7842. [[CrossRef](#)]
32. Samal, S.; Rahul, M.R.; Kottada, R.S.; Phanikumar, G. Hot deformation behaviour and processing map of Co-Cu-Fe-Ni-Ti eutectic high entropy alloy. *Mater. Sci. Eng. A* **2016**, *664*, 227–235. [[CrossRef](#)]
33. Rogal, Ł.; Morgiel, J.; Świątek, Z.; Czerwiński, F. Microstructure and mechanical properties of the new Nb<sub>25</sub>Sc<sub>25</sub>Ti<sub>25</sub>Zr<sub>25</sub> eutectic high entropy alloy. *Mater. Sci. Eng. A* **2016**, *651*, 590–597. [[CrossRef](#)]
34. He, F.; Wang, Z.J.; Cheng, P.; Wang, Q.; Li, J.J.; Dang, Y.Y.; Wang, J.C.; Liu, C.T. Designing eutectic high entropy alloys of CoCrFeNiNb<sub>x</sub>. *J. Alloy. Compd.* **2016**, *656*, 284–289. [[CrossRef](#)]
35. Guo, S.; Ng, C.; Liu, C.T. Anomalous solidification microstructures in Co-free Al<sub>x</sub>CrCuFeNi<sub>2</sub> high-entropy alloys. *J. Alloy. Compd.* **2013**, *557*, 77–81. [[CrossRef](#)]
36. Tan, Y.M.; Li, J.S.; Wang, J.; Kou, H.C. Seaweed eutectic-dendritic solidification pattern in a CoCrFeNiMnPd eutectic high-entropy alloy. *Intermetallics* **2017**, *85*, 74–79. [[CrossRef](#)]
37. Jin, X.; Zhou, Y.; Zhang, L.; Du, X.Y.; Li, B.S. A novel Fe<sub>20</sub>Co<sub>20</sub>Ni<sub>41</sub>Al<sub>19</sub> eutectic high entropy alloy with excellent tensile properties. *Mater. Lett.* **2018**, *216*, 144–146. [[CrossRef](#)]
38. Jiang, H.; Qiao, D.X.; Lu, Y.P.; Ren, Z.; Cao, Z.Q.; Wang, T.M.; Li, T.J. Direct solidification of bulk ultrafine-microstructure eutectic high-entropy alloys with outstanding thermal stability. *Scr. Mater.* **2019**, *165*, 145–149. [[CrossRef](#)]
39. Jiang, H.; Jiang, L.; Qiao, D.X.; Lu, Y.P.; Wang, T.M.; Cao, Z.Q.; Li, T.J. Effect of Niobium on Microstructure and Properties of the CoCrFeNb<sub>x</sub>Ni High Entropy Alloys. *J. Mater. Sci. Technol.* **2016**, *33*, 712–717. [[CrossRef](#)]
40. Bento, J.L.; Brown, E.; Woltornist, S.J.; Adamson, D.H. Thermal and electrical properties of nanocomposites based on self-assembled pristine graphene. *Adv. Funct. Mater.* **2017**, *27*, 1604277. [[CrossRef](#)]
41. Sondheimer, E.H. Mean free path of electrons in metals. *Adv. Phys.* **1952**, *1*, 1–42. [[CrossRef](#)]
42. Kaya, H.; Büyük, U.; Çadırlı, E.; Maraşlı, N. Measurements of the microhardness, electrical and thermal properties of the Al–Ni eutectic alloy. *Mater. Des.* **2012**, *34*, 707–712. [[CrossRef](#)]
43. Chou, H.P.; Chang, Y.S.; Chen, S.K.; Yeh, J.W. Microstructure, thermophysical and electrical properties in Al<sub>x</sub>CoCrFeNi (0 ≤ x ≤ 2) high-entropy alloys. *Mater. Sci. Eng. B* **2009**, *163*, 184–189. [[CrossRef](#)]
44. Sui, Y.; Gao, S.; Chen, X.; Qi, J.; Yang, F.; Wei, F.; He, Y.; Meng, Q.K.; Sun, Z. Microstructures and electrothermal properties of Al<sub>x</sub>CrFeNi multi-component alloys. *Vacuum* **2017**, *144*, 80–85. [[CrossRef](#)]



45. Cassinelli, M.; Muller, S.; Voss, K.O.; Trautmann, C.; Volklein, F.; Gooth, J.; Nielsch, K.; Toimil-Molares, M.E. Influence of surface states and size effects on the Seebeck coefficient and electrical resistance of  $\text{Bi}_{1-x}\text{Sb}_x$  nanowire arrays. *Nanoscale* **2017**, *9*, 3169–3179. [[CrossRef](#)] [[PubMed](#)]
46. Mingo, N.; Hauser, D.; Kobayashi, N.P.; Plissonnier, M.; Shakouri, A. Nanoparticlein alloy approach to efficient thermoelectrics: Silicides in sige. *Nano Lett.* **2009**, *9*, 711–715. [[CrossRef](#)]
47. Shackelford, J.F.; Alexander, W. (Eds.) *CRC Materials Science and Engineering Handbook*, 3rd ed.; CRC Press: Boca Raton, FL, USA, 2000.
48. Lide, D.R. (Ed.) *CRC Handbook of Chemistry and Physics*, 84th ed.; CRC Press: Boca Raton, FL, USA, 2003.



© 2020 by the authors. Licensee MDPI, Basel, Switzerland. This article is an open access article distributed under the terms and conditions of the Creative Commons Attribution (CC BY) license (<http://creativecommons.org/licenses/by/4.0/>).